Chem Soc Rev

Multifunctional π-expanded oligothiophene macrocycles

Journal:	*Chemical Society Reviews*
Manuscript ID:	CS-TRV-05-2015-000388.R1
Article Type:	Tutorial Review
Date Submitted by the Author:	25-Jun-2015
Complete List of Authors:	Iyoda, Masahiko; Tokyo Metropolitan University, Department of Chemistry, Graduate School of Science and Engineering Shimizu, Hideyuki; Tokyo Metropolitan University, Department of Chemistry, Graduate School of Science and Engineering

Chem Soc Rev

RSCPublishing

TUTORIAL REVIEW

Multifunctional π-expanded oligothiophene macrocycles

Cite this: DOI: 10.1039/x0xx00000x

Masahiko Iyoda* and Hideyuki Shimizu

Received 00th January 2012,
Accepted 00th January 2012

DOI: 10.1039/x0xx00000x

www.rsc.org/

This tutorial review summarizes recent progress in the design, synthesis, and multifunctional properties of fully conjugated macrocyclic π-systems. We focus on the π-expanded oligothiophene macrocycles after a short survey of macrocyclic conjugated loops and belts such as [*n*]cycloparaphenylenes, cyclic [*n*]para-phenylacetylenes, [4]cyclo-2,8-crysenylenes, and cyclo[*n*]thiophenes. Fully conjugated π-expanded oligothiophene macrocycles possess shape-persistent but sometimes pliable π-frames, and electronic and optoelectronic properties of the macrocycles largely depend on the π-systems inserted into the oligothiophene macrocycles. Among them, the π-expanded oligothiophene macrocycle composed of 2,5-thienylenes, ethynylenes, and vinylenes is one of the most widely applicable macrocycles for constructing multifunctional π-systems. These π-expanded oligothiophene macrocycles from small to very large ring sizes can be prepared via a short step procedure, and their various solid state structures can be determined by X-ray analysis. Since these macrocycles have inner and outer domain, specific information concerning structural, electronic, and optical properties is expected. Furthermore, π-expanded oligothiophene macrocycles with alkyl substituents exhibit various morphologies depending on nanophase separation of molecules, and morphological change is available for molecular switch.

Key learning points

(1) Nanosized conjugated macrocycles are fundamentally important due to the novel structures, properties, and functions.
(2) Fully unsaturated macrocycles are regarded as models for infinitely conjugated π-systems with inner cavities, and exhibit unique optical, electronic, and magnetic behavior.
(3) Macrocycles have interior and exterior sites, and site-specific substitution at both or either site can afford attractive structures, such as 1D, 2D, and 3D supramolecular nanostructures.
(4) π-Expanded oligothiophene macrocycles have shape-persistent frameworks with medium to large inner cavities and incorporate from small to large molecules as a guest.
(5) Large π-expanded oligothiophene macrocycles exhibit marked nonlinear optical properties and behave like the natural light-harvesting system.

1. Introduction

Cyclic benzenoid and nonbenzenoid conjugated molecules have important roles in chemical sciences.[1] As synthetic and analytical techniques have advanced recently, several fully conjugated cyclic molecules have been developed to investigate cyclic conjugation in relation to the Hückel and Möbius aromaticity,[2] to examine three-dimensional conjugation in hoop- and belt-shaped molecules,[3] and recently to create molecular machines, sensors, and switches utilizing their electric and optical properties.[4] Among all of the different conjugated cyclic molecules, fully conjugated macrocycles with precisely defined diameters are regarded as being formally infinite π-conjugated systems free from the effect of terminal groups, and thus these π-systems have attracted considerable attention owing to their unusual optical, electronic, and magnetic properties arising from this effective cyclic conjugation. Large fully conjugated macrocycles sometimes show no diatropic (aromatic) or paratropic (antiaromatic) ring current. These macrocycles, however, also exhibit remarkable photophysical properties based on their conjugation and ring size.

Conjugated macrocycles have shape-persistent inner cavities, and small molecules or ions are incorporated in the cavity as guests to produce interesting supramolecular structures. Moreover, large macrocycles having round-shaped inner cavities of 10–11 Å can incorporate large molecules, such as fullerene C_{60} or C_{70} to produce inclusion complexes. These supramolecular complexes are stabilized by concave–convex π–π interaction, charge-transfer (CT) interaction, CH/π interaction, and van der Waals interaction. In the case of giant macrocycles with cavities >12 Å, the flexibility of the macrocycles increases, and the cavity size becomes too large to incorporate molecules. Even though the molecular structure of these nanoscale macrocycles is sometimes not unambiguously determined, they show remarkable photophysical properties and nonlinear optical behavior.

On account of nanophase separation induced by interior and exterior sites, macrocycles with shape-persistent, noncollapsible, and fully π-conjugated backbones can assemble into columnar one-dimensional (1D) nanotubes,[5] two-dimensional (2D) porous networks and lamellar alignments on surfaces,[6] and three-dimensional (3D) inclusion complexes in the solid state (Fig. 1).[3,7] In

the case of redox-active macrocycles, therefore, these macrocycles change their charge and shape upon reduction or oxidation, and the site-specific character of macrocycles can be adjusted at both their inner and outer sites. Although polymorphism of functional macrocycles has not yet been fully elucidated owing to the lack of suitable examples, nanostructured polymorphs can be employed in a wide range of applications.[8]

This tutorial review will discuss the extension of cyclic conjugation, redox properties and conducting behavior, guest molecule incorporation in the inner cavity, polymorphism of functional macrocycles, and nonlinear optical properties of π-expanded oligothiophene macrocycles.

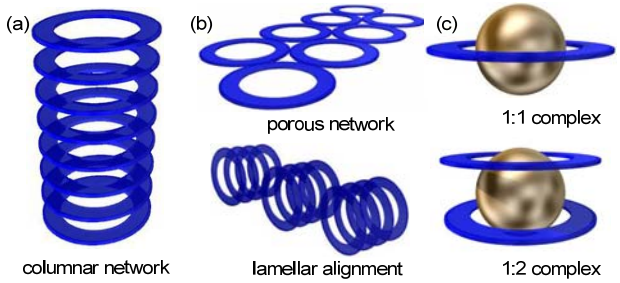

Fig. 1 Possible supramolecular nanostructures of (a) 1D-, (b) 2D-, and (c) 3D-alignments of conjugated macrocycles.

1. Conjugated macrocycles

2.1 Oligophenylene macrocycles

During the past two decades, three π-conjugated macrocyclic loops and belts have been reported (Fig. 2). In 1996, Kawase and Oda first reported the synthesis of cyclic [6]- and [8]paraphenyleneacetylenes (**[6]CPPA** and **[8]CPPA**).[9] They also reported the synthesis of **[7]CPPA**, **[9]CPPA**, and the related naphthalene derivatives.[3] In 2008, Jasti, Bertozzi, and co-workers reported the synthesis of [9]-, [12]-, and [18]cycloparaphenylenes (**[9]CPP**, **[12]CPP**, and **[18]CPP**).[10] These **CPP**s exhibited unique emission behavior, and the smaller **CPP**s have longer wavelength emission maxima. Recently, Isobe reported tubular macrocycles, [4]cyclo-2,8-crysenylene (**[4]CC$_{2,8}$**) and its derivatives, possessing sp^2-networks of single wall carbon nanotube.[11]

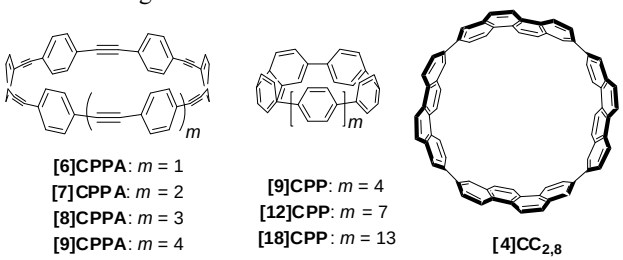

Fig. 2 Structures of **[*n*]CPPA**s, **[*n*]CPP**s, and **[4]CC$_{2,8}$**.

Quite recently, the synthesis of **CPP**s were developed very rapidly and extensively by the groups of Itami,[12] Yamago,[13] Jasti,[14] and Müllen,[15] independently, and **[5]**–**[16]CPP**s and their derivatives were newly synthesized to explore characteristic properties. **CPP**s are structural units of fullerenes and armchair carbon nanotubes (**CNT**s), affording the corresponding cationic and anionic species by oxidation and reduction, respectively. Interestingly, **[8]CPP^{2+}** showed in-plane aromaticity with 30π-electrons.[16,17] Furthermore, the cavity of the **CPP**s acts as a host for π-conjugated molecules, and C_{60} was selectively encapsulated by **[10]CPP**, forming a 1 : 1 complex, **[10]CPP**⊃C_{60} (Fig. 3).[18,19] In the case of **[6]CPPA**, this molecule takes C_{60} in the cavity to form **[6]CPPA** ⊃ C_{60}. Furthermore, since **[9]CPPA** incorporates **[6]CPPA** to afford **[9]CPPA**⊃**[6]CPPA**, **[6]CPPA**⊃C_{60} is encapsulated by **[9]CPPA** to produce an onion-type complex **[9]CPPA**⊃**[6]CPPA**⊃C_{60} (Fig. 3).[20] **[4]CC$_{2,8}$** having two hexyl groups at 6 and 12 positions strongly encapsulates C_{60} with an extremely high binding constant (log K_a = 11.5 in toluene), and C_{60} rolls anisotropically in a bearing on the molecular scale.[11]

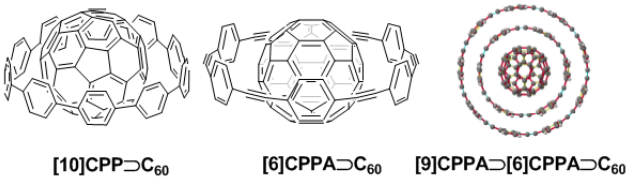

Fig. 3 Inclusion complexes of **[10]CPP** and **[6]CPPA** with C_{60} and onion-type complex **[9]CPPA**⊃**[6]CPPA**⊃C_{60}.

2.2 Macrocyclic cyclo[*n*]thiophenes

The pioneering study on the synthesis of cyclo[*n*]thiophenes **C12T**, **C14T**, and **C16T** by Bäuerle *et al.* employed copper-mediated coupling for the construction of macrorings, and oxidative coupling of **1** or **2** yielded **3** and **5** or **4** and **6**, respectively.[21,22] The reactions of **3**, **4**, and **5** with sodium sulfide afforded **C12T**, **C16T**, and **C18T**, respectively (Scheme 1). Computational studies predicted that *syn*-**C8T**–**C12T** possess nearly planar structures. In *syn*-conformation, however, large **C*n*T**s lose their nearly planar ring shape and bent significantly for n > 14. From scanning tunnelling microscope (STM) measurements, **C12T** self-assembled in a hexagonal close-packed monolayer at the solid–liquid interface. Moreover, a 2D porous network of **C12T** formed a two-component system with C_{60}.[23] The STM images showed 1:1 donor/acceptor complexes and a 3D supramolecular assembly.

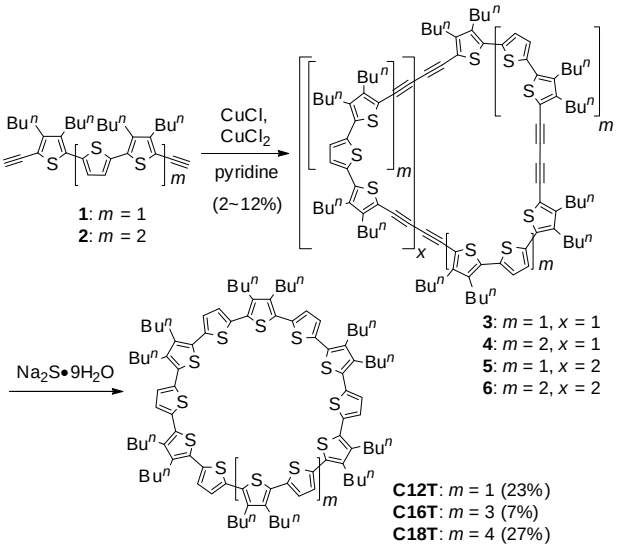

Scheme 1 Synthesis of fully a-conjugated cyclo[*n*]thiophenes **C12T**, **C16T**, and **C18T**.

Bäuerle *et al.* developed a new method of synthesizing cyclo[8]thiophene (**C8T**) via platinum intermediate **7** (Scheme 2).[24]

The C–C bond formation through reductive elimination led to the strained cyclodimeric terthiophene-diyne **8**, which was converted into **C8T**. Although **C8T** can be expected to possess a strained planar structure with a high donor ability, no structural information and redox behavior were reported.

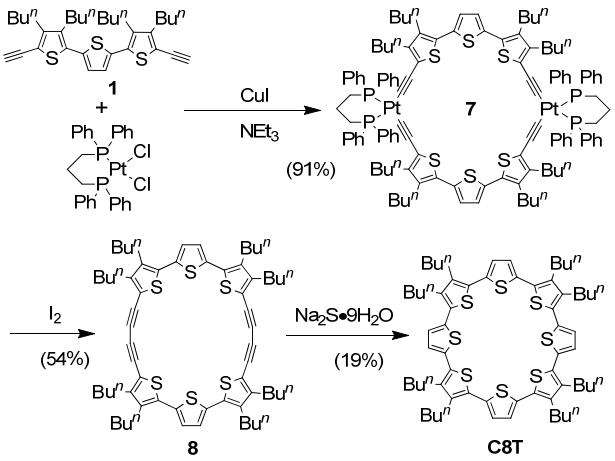

Scheme 2 Synthesis of **C8T** via platinum complex **7**.

Recently, the same research group reported a new approach to synthesize highly symmetric macrocyclic oligothiophenes **C10T**–**C35T**, which have interesting optoelectronic and supramolecular properties (Scheme 3).[25] These macrorings were prepared via multinuclear macrocyclic Pt^{II} complexes **10** and **11**. The high symmetry of the cyclic structures of **C10T**–**C35T** influences their photophysical properties: the absorption maxima corresponding to an $S_0 \rightarrow S_2$ electronic transition were red-shifted and showed a hyperchromic effect with an increase in the ring size. The X-ray analysis of **C10T** showed a nearly circular structure with inner diameters of ca. 1.0 nm, and adjacent thiophene units are twisted up and down by 26–34º to release the ring strain. The very low oxidation potential (0.03 V vs Fc/Fc^+) of the smallest cycle **C10T** was attributed to a high HOMO level due to the *syn* conformation of the thiophene units. Interestingly, two-electron oxidation of **C10T** formed a two-polaron structure (polaron-pair) $\mathbf{C10T}^{2(\cdot+)}$.[26]

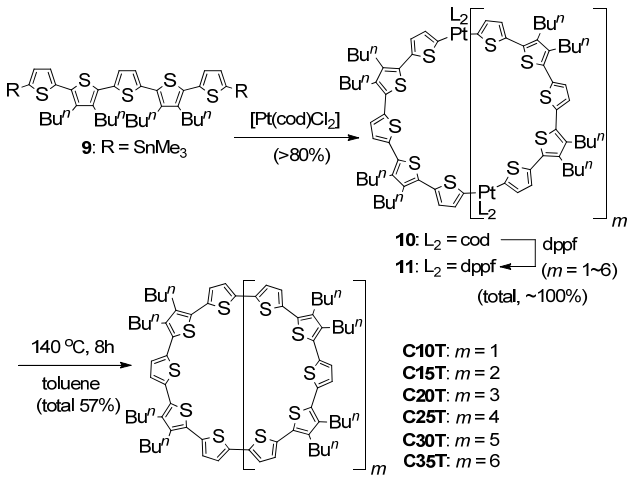

Scheme 3 Synthesis of **C10T**–**C35T**.

Quite recently, Sannicolò and co-workers reported chiral macrocyclic oligothiophenes **13** (15%) and **14** (8%) by chemical oxidation of **12** with $FeCl_3$ (Fig. 4).[27] These macrocycles showed chiroptical properties, circularly polarized luminescence effects, and enantiorecognition ability. Cyclic octithiophene **16** containing two β,β'-linkages was synthesized from cyclic platinum complex **15** (>68%).[28] The fluorescence spectra of the nonplanar **16** showed a redshift as compared to the corresponding quaterthiophene owing to the large structural change in the excited state.

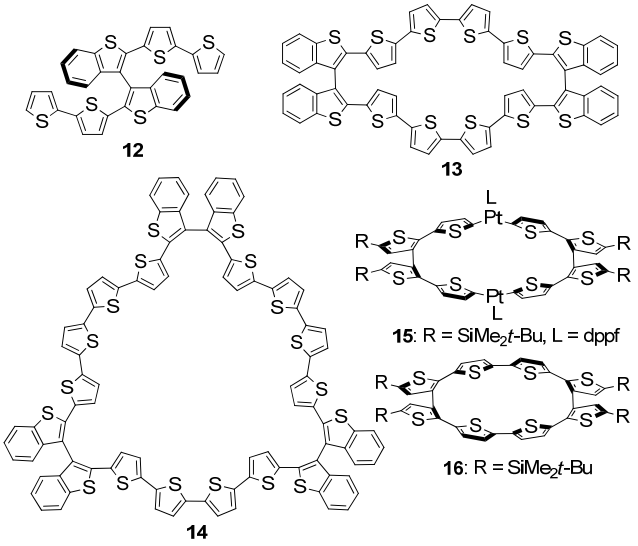

Fig. 4 Cyclic oligothiophenes **13**, **14**, and **16** and their precursors **12** and **15**.

3. π-Expanded oligothiophene macrocycles

3.1 Planar and nonplanar macrocycles

Fully conjugated π-expanded oligothiophene macrocycles are a family closely related to redox-active oligothiophene macrocycles such as **C[*n*]T**s, exhibiting potential optoelectronic application to organic light-emitting diodes (OLED), organic field-effect transistors (OFET), organic solar cells, and many others.[22] These π-expanded macrocycles possess shape-persistent π-frames, and electric and optoelectronic properties of the macrocycles largely depend on the inserted π-systems to the parent oligothiophene macrocycles. Although [*n*]cycloparaphenylenes (**CPP**s), [*n*]paraphenyleneacetylenes (**CPPA**s), and [4]cyclo-2,8-crysenylenes ($\mathbf{CC_{2,8}}$) possess a 3D hoop-shaped conjugation with p-orbitals parallel to the macroring, p-orbitals of **C[*n*]T**s containing α,α'-linkages are aligned perpendicular to the planar macroring. On the other hand, cyclic oligothiophenes **13**, **14**, and **16** containing β,β'-linkage adopt a twisted structure around the β,β'-linkage (Fig. 4).

Among π-expanded oligothiophene macrocycles, Marsella and co-workers reported the synthesis of **17** containing two rings with potential use as single-molecule electrochemical actuators (Fig. 5).[29] Cyclooctatetraene (COT) is oxidized to give the planar COT^{2+}, and distance d_1 (3.142 Å) in the tub form increases to distance d_2 (3.407 Å). Therefore, a large redox-induced conformational change between twisted and planar topologies, associated with 18% change in distance, was predicted for the four-electron oxidation of **17** on the basis of DFT calculations. Very recently, cyclo-1,4-phenylene-2',5'-thienylenes (**CPT**s) were synthesized by Itami and co-workers

using a synthetic method similar to **CPP**s.[30] X-ray analysis revealed that **[4]CPT**·2cyclohexane adopts a C_{4v}-symmetric truncated cone shape with tubular stacking along the *c*-axis. Hasegawa and co-workers reported the synthesis of thiacalix[n]dithienothiophenes **19a-c** by a simple Pd-catalyzed coupling reaction of **18** in the presence of $(n\text{-}Bu_3Sn)_2S$.[31] Although X-ray analysis of **19a,b** exhibited a twisted 3D structure, electrochemically generated cationic species **19a-c**$^{\cdot+}$ showed a 3D delocalization of π-electrons.

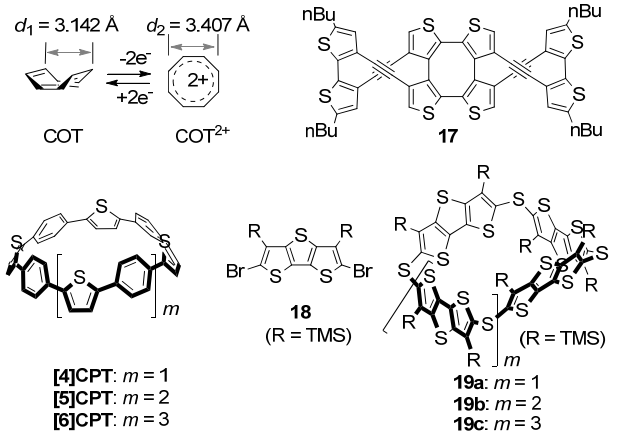

Fig. 5 Nonplanar π-expanded oligothiophene macrocycles **17**, [*n*]**CPT**s (*m* = 1-3), and **19a-c**.

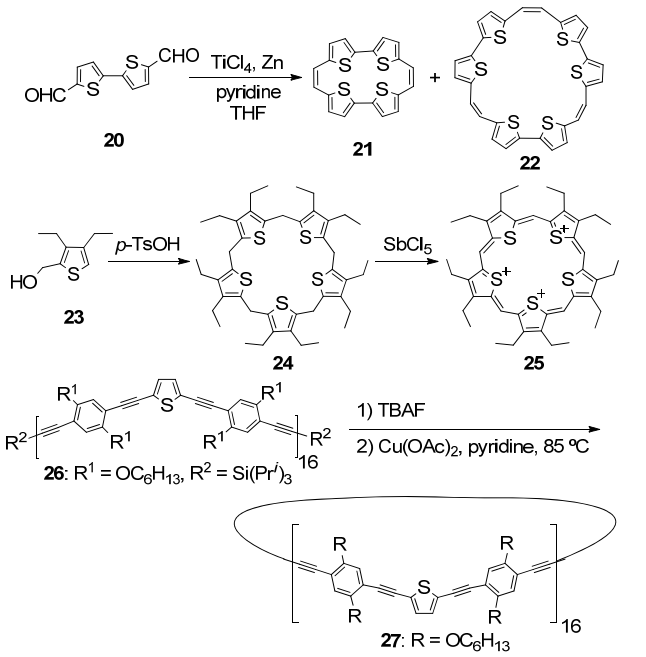

Scheme 4 Synthesis of π-expanded oligothiophene macrocycles **21**, **22**, **25**, and **27**.

Various synthetic methods can be employed for the synthesis of π-expanded oligothiophene macrocycles. As shown in Scheme 4, Cava and co-workers reported the intermolecular cyclization of dialdehyde **20** by using McMurry coupling to produce **21** and **22**.[32] The sulfur analogue **25** of 22π-pentaphyrin was reported by Vogel and co-workers.[33] Mayor and Didschies synthesized one of the largest macrocycles, **27**, with a diameter of 11.8 nm by using intramolecular Eglington coupling.[34] **27** has a fully conjugated periphery composed of ethynylene, butadiynylene, 2,5-thienylene, and 1,4-phenylene units.

Large planar macrocycles stack through π-π interaction on the surface to form a lamellar structure favourable for charge-carrier mobility. Aso and co-workers reported the synthesis and OFET performance of rectangular macrocycle **28** with benzothiophene units at the corner position (Fig. 6).[35] A film fabricated by spin-coating exhibited a hole mobility with a maximum value of 7.3×10^{-3} $cm^2V^{-1}s^{-1}$. 2D-supramolecular structures comprised of **29** and its co-deposition with C_{60} on HOPG were investigated by Höger, Freyland, and co-workers (Fig. 6).[36] High-resolution STM investigation of monolayers revealed that the presence of two individual bithiophene units as well as the size of the macrocycle led to the formation of a superstructure with a 1:2 stoichiometry. The fullerene units were located around the periphery of the bithiophene units, thus indicating the donor-acceptor interaction between C_{60} and the electron-rich bithiophene units of **29**.

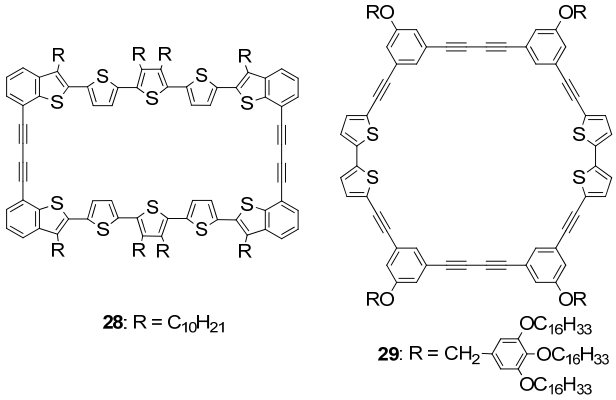

Fig. 6 Planar π-expanded oligothiophene macrocycles **28** and **29**.

3.2 Macrocycles composed of 2,5-thienylene, ethynylene, and vinylene units

A series of π-expanded oligothiophene macrocycles composed of 2,5-thienylene, ethynylene, and vinylene units has been synthesized using a modified McMurry coupling reaction of dialdehydes **30** as the key step (Scheme 5).[1,37] Although repeated and thus monotonic synthetic procedures are inevitable for forming large cyclic structures, this method can be effectively applied to construct small **6T6A**, medium **10T8A**, giant **30T25A**, and other related macrorings. π-Expanded oligothiophenes with long alkyl chains can be envisaged as self-assembling into nanostructures such as nanowires, nanotubes, and nanoparticles using π-π and van der Waals interactions unlike macrocyclic oligophenylenes and oligopyrroles.[38] Thus, reducing the dimensionality of macrocycles having non-hydrogen-bonding interactions from a 3D crystal structure into 1D or 2D structures leads to the self-assembling nanostructures. Furthermore, these oligothiophene macrocycles show a good mobility of ring electrons and hence strong cyclic conjugation owing to fairly planar structures of 2,5-thienylene, ethynylene, and vinylene units. All oligothiophene macrocycles are stable reddish orange crystalline or amorphous powders and soluble in common organic solvents, except for methanol. Therefore, π-expanded oligothiophene macrocycles are an ideal system to investigate relationship between cyclic conjugation and photophysical behavior. Furthermore, these macrocycles can show a novel ring size effect on chemical and physical properties.

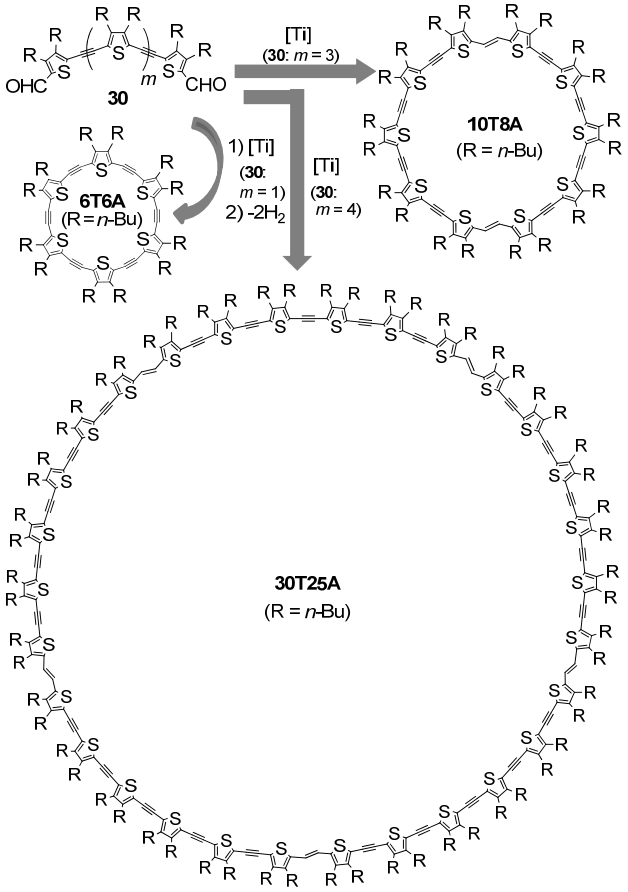

Scheme 5 Typical π-expanded macrocyclic oligothiophenes **6T6A**, **10T8A**, and **30T25A**.

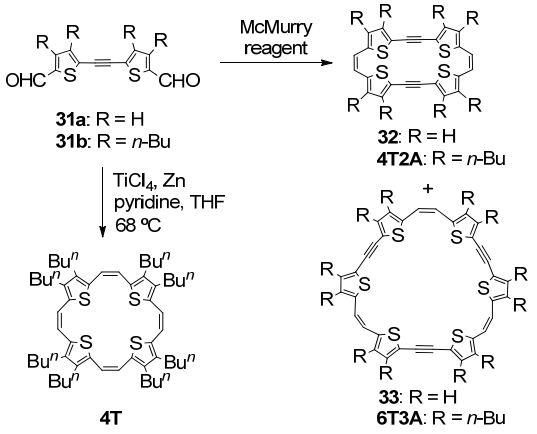

Scheme 6 McMurry coupling of **31a** and **31b**.

Kawase and co-workers reported that the coupling of **31a** with a McMurry reagent prepared from $TiCl_3(DME)_{1.3}$–Zn(Cu) in DME gave the dimer **32** in only trace amounts together with the corresponding trimer (10–15%) (Scheme 6).[39] On the other hand, the reaction of **31b** with a McMurry reagent prepared from $TiCl_4$–Zn in gently refluxing THF–pyridine at 60 ºC produced **4T2A** (15%) and **6T3A** (13%), and the McMurry coupling of **31b** under similar conditions at 68 ºC formed **4T** as a major product.[40] Therefore, selection of the reaction condition of the McMurry coupling is the key to the synthesis of macrocyclic oligothiophenes.

Intramolecular pinacol coupling of **34** with a low-valent vanadium complex produced the corresponding cyclic 6-mer diol **35**.[41] However, a Corey-Winter reaction of the diol afforded a complex mixture of products (Scheme 7). Since **6T5A** is a strained compound, **6T5A** or its precursors could not survive under the Corey-Winter conditions.

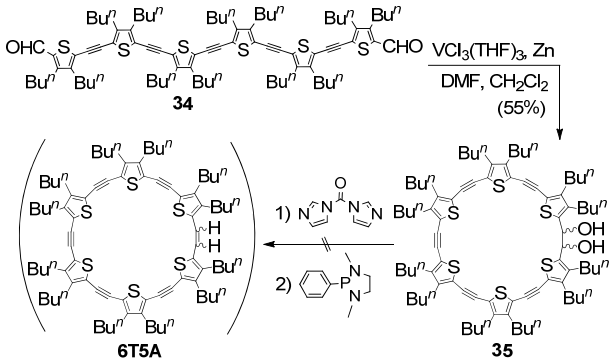

Scheme 7 Attempted synthesis of **6T5A** starting from **34**.

The synthesis of oligothiophene 6-mer **6T4A** and related higher oligomers was carried out by using a modified McMurry reaction, as shown in Scheme 8.[42] Reaction of the dialdehyde **36** composed of three 2,5-thienylene and two ethynylene units with a low-valent titanium reagent proceeded smoothly to mainly produce cyclic dimer **6T4A** (35%) together with cyclic trimer **9T6A** (5.5%) and cyclic tetramer (1.5%). Although the formation of a small amount of cyclic pentamer was observed, no linear di-, tri-, tetra-, or pentamers were isolated from the reaction mixture except for higher polymers. Cyclic dimer **6T4A** was converted to cyclo[6](3,4-dibutyl-2,5-thienylene-ethynylene) **6T6A** by using a bromination-dehydrobromination procedure (45%).

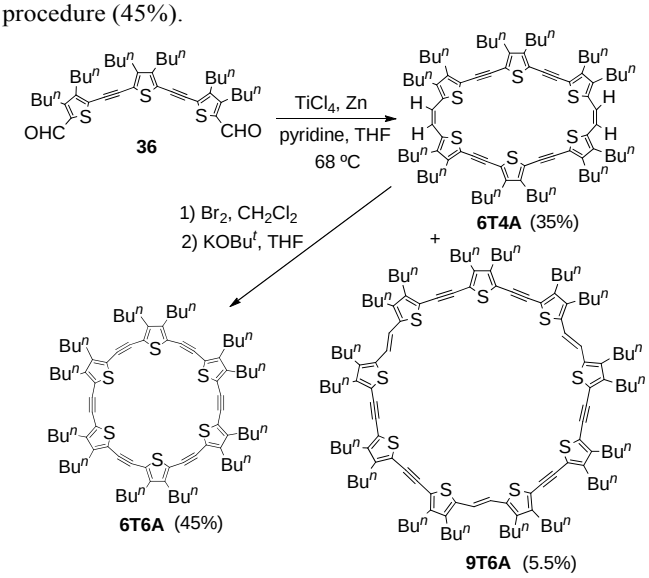

Scheme 8 Synthesis of **6T4A**, **9T6A**, and **6T6A**.

To synthesize **8T6A**, a McMurry coupling reaction of **37** composed of four 2,5-thienylene and three ethynylene units was carried out under very high-dilution conditions in the dark to produce *Z,Z*-**8T6A** (35%) and *E,E*-**8T6A** (1%) with a trace amount of the corresponding 12-mer (Scheme 9).[43] Although *E,E*-**8T6A** is more stable than *Z,Z*-**8T6A**, the reaction mainly afforded *Z,Z*-**8T6A** as a kinetic product, reflecting the

stereochemistry of the bis(*erythro*-diol) intermediate. *E*,*E*-**8T6A** easily isomerizes to *Z*,*Z*-**8T6A** in ambient light, whereas *Z*,*Z*-**8T6A** slowly isomerizes to *E*,*E*-**8T6A** under UV irradiation (photochromism).

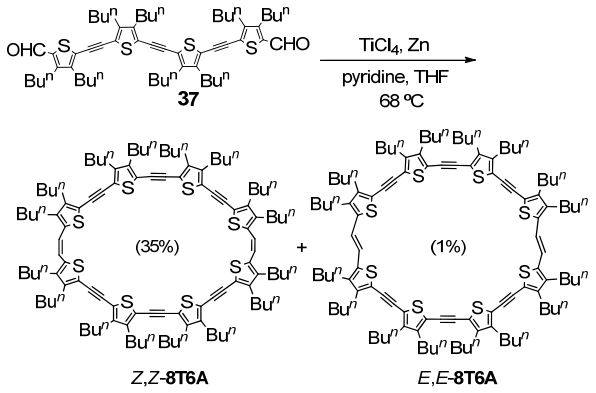

Scheme 9 Synthesis of *Z*,*Z*-**8T6A** and *E*,*E*-**8T6A**.

In case of cyclo[8](3,4-dibutyl-2,5-thienylene-ethynylene) **8T8A**, this compound was synthesized by intramolecular Sonogashira cyclization of linear ethynylbromide **38** composed of eight 2,5-thienylene and seven ethynylene core units (14%) (Scheme 10). Furthermore, bromination of *E*,*E*-**8T6A** or *Z*,*Z*-**8T6A**, followed by dehydrobromination with potassium *t*-butoxide, produced **8T8A** in 21% overall yield.[43]

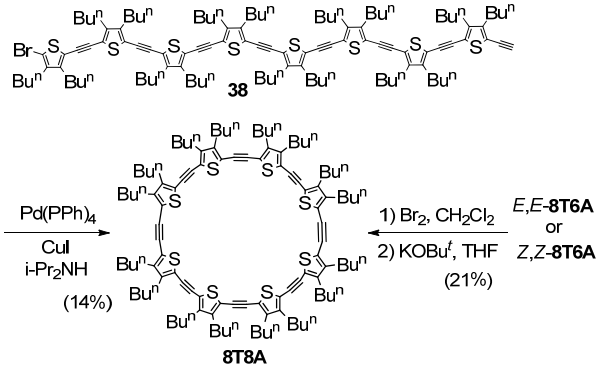

Scheme 10 Synthesis of **8T8A** using intramolecular cyclization or bromination–dehydrobromination procedure

For the synthesis of **10T8A**–**30T24A**, the coupling of **39** was carried out using $TiCl_4$–Zn in THF–pyridine under normal dilution conditions (Scheme 11).[44] This reaction produced a mixture of cyclic oligomers, which can be separated easily by gel permeation chromatography on polystyrene with toluene or chloroform as an eluent to afford the 30π–**10T8A** (39%), 90π–**15T12A** (9.4%), 120π–**20T16A** (6.2%), 150π–**25T20A** (3.9%), and 180π–**30T24A** (2.3%), together with a 1:3 mixture of the *E*,*Z*- and *Z*,*Z*-isomers of **10T8A** (7%) in total 65.5 % yield (Scheme 11). Since **10T8A** crystallizes from chloroform-heptane, pure **10T8A** can be isolated from the mixture of stereoisomers. Variable temperature (VT) NMR spectroscopic studies revealed that **10T8A**–**30T24A** show symmetrical D_{nh} structures even at -60 ºC, reflecting a rapid conformational change in solutions. Although this reaction produces a mixture of cyclic oligomers **10T8A**–**30T24A**, the yield of **10T8A** is a permissive range for synthetic chemists. Furthermore, the less easy-obtainable higher oligomers **15T12A**–**30T24A** can also be synthesized by a one-step procedure. Intramolecular Sonogashira cyclization of **40** or bromination of **10T8A**, followed by dehydrobromination with potassium *t*-butoxide, produced **10T10A** in 40 and 36% overall yield, respectively.

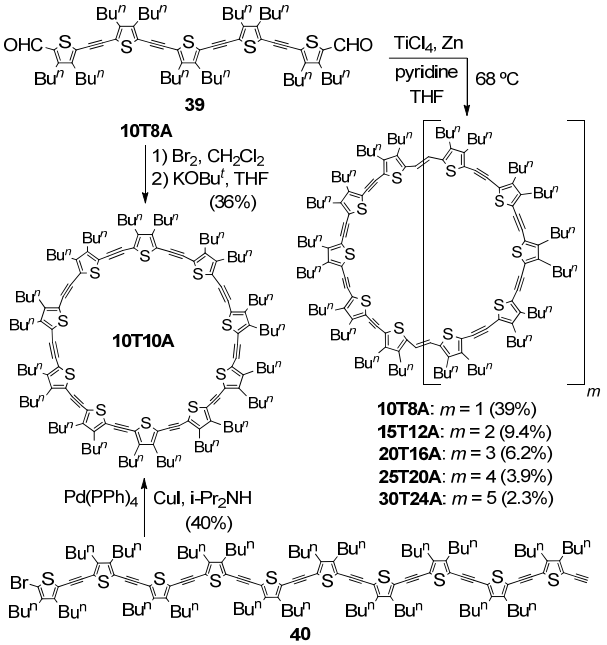

Scheme 11 Synthesis of **10T8A**–**30T24A** and **10T10A**.

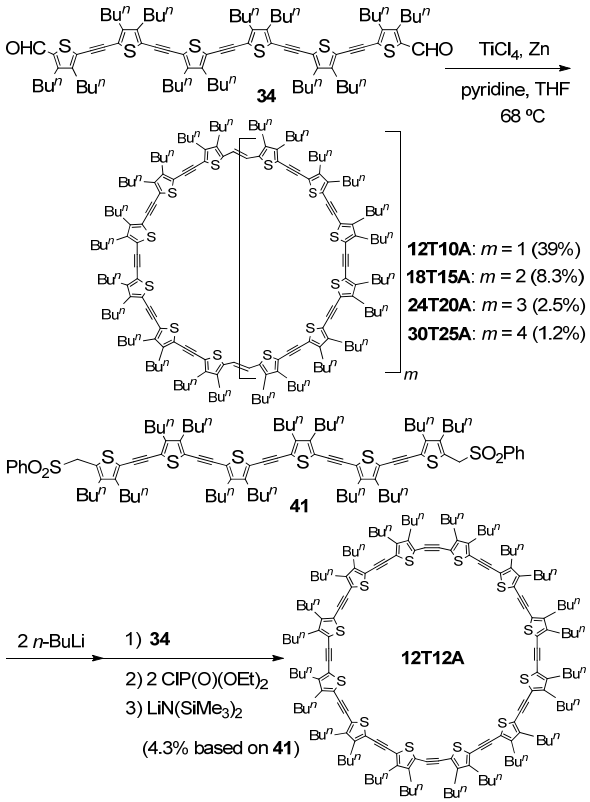

Scheme 12 Synthesis of **12T10A**–**30T25A** and **12T12A**.

Similarly to the synthesis of **10T8A**–**30T24A**, the intermolecular McMurry coupling of **34** with $TiCl_4$–Zn in THF–pyridine under normal dilution conditions produced the 72π–**12T10A**, 108π–**18T15A**, 144π–**24T20A**, and 180π–**30T25A** in 39, 8.3, 2.5, and 1.2% yields, respectively, together

with a small amount of the *E*,*Z*- and *Z*,*Z*-isomers of **12T10A** (Scheme 12).[45] Furthermore, the 216π-hexamer **36T30A** was isolated in 0.2% yield, though **36T30A** was not fully characterized. For the synthesis of **12T12A** by using 'double elimination procedure',[46] the sulfone dianion prepared from **41** was reacted with the dialdehyde **34** (1 equiv). The adduct formed from **41** and **34** was reacted with diethyl chlorophosphate (2 equiv), followed by treatment with lithium hexamethyldisilazide (4 equiv) producing **12T12A** in 4.3% overall yield.

For the synthesis of π-expanded oligothiophene macrocycles composed of 2,5-thienylene, ethynylene, and vinylene units, McMurry coupling reaction is a versatile tool, and **6T4A**, **8T6A**, **10T8A**, and **12T10A** were synthesized in 18, 24, 19, and 16% overall yields, respectively, in gram scale in 6-8 steps from commercially available 3,4-dibutylthiophene. For isolating **6T4A**, **8T6A**, **10T8A**, and **12T10A**, all products were first recrystallized from crude mixtures, and the residues were separated by gel permeation chromatography (GPC).

3.3 Crystal structures of π-expanded oligothiophene macrocycles

The molecular structures of **32**, **4T2A**, **6T4A**, **6T6A**, **10T8A**, and **12T10A** have been determined by X-ray analysis (Fig. 7 to 11). As shown in Fig. 7a, **4T2A** has an extremely twisted structure,[40] although the corresponding unsubstituted molecule **32** is planar (Fig. 8).[39] The ^{1}H NMR spectrum of **4T2A** at room temperature was consistent with a symmetrical D_{2h} structure, and hence **4T2A** may undergo a rapid conformational change in solution. The crystal packing of **4T2A** having eight butyl groups may demand to take a twisted structure (Fig. 7b). The interatomic S···S distance (3.262 Å) in **4T2A** is 12% shorter than the sum of S···S van der Waals radii (3.70 Å), whereas the similar distances (3.014 and 3.025 Å) in **32** are 18% shorter than the sum of van der Waals radii. Therefore, π–π stacking interaction in the crystal lattice overcomes destabilization of the planar structure in **32**. It is noteworthy that a flexible macroring easily forms various crystal structures depending on weak interactions in the crystal lattice.

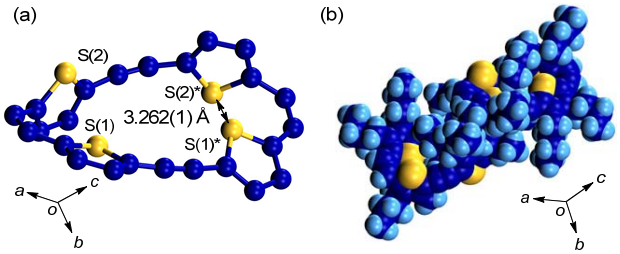

Fig. 7 X-ray structure of **4T2A**. (a) Molecular structure with butyl groups and hydrogen atoms omitted for clarity. (b) Entangled packing structure.

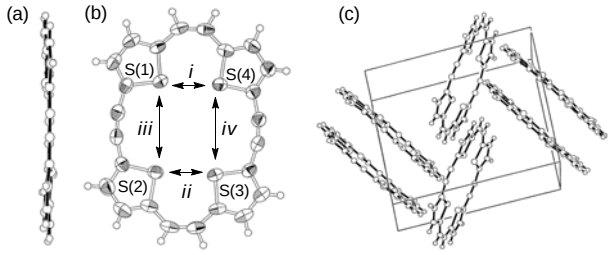

Fig. 8 X-ray structure of **32**. (a) Side view, (b) Top view, and packing structure. Interatomic S···S distance (Å): *i* 3.014(2), *ii* 3.025(2), *iii* 4.567(3), *iv* 4.544(3).

DFT calculations on unsubstituted **6T4A** predicted a planar structure. However, **6T4A** lies on a crystallographic center of symmetry (Fig. 9a), and the macroring adopts a nonplanar twisted conformation.[42] The S(1)···S(1)* and S(2)···S(3) distances are 5.8272(16) Å and 3.2456(12) Å, respectively, and the latter is similar to that of **4T2A** (Fig. 7a). In the molecular packing of **6T4A**, one set of butyl groups lie above and below the ring, filling the pore of the neighboring ring, and the other set of butyl groups are arranged laterally without intermolecular interactions (Fig. 9b). Therefore, there are no significant intermolecular π–π interactions between the thiophenes of **6T4A**. In contrast to the crystal structure of **6T4A**, VT ^{1}H NMR spectroscopy in $CDCl_3$ indicated that the structure was D_{2h}-symmetric, and there were no spectral changes at low temperature. Interestingly, **6T6A** crystallized with a hexane molecule located in the center of the cavity (Fig. 9c). The ring has a crystallographic inversion center at the center of the macrocycle. As expected, the π-framework of **6T6A** is fairly planar and circular in shape. The averaged S(1)···S(1*), S(2)···S(2*), and S(3)···S(3*) distances were found to be 9.85 Å, which is considerably close to the corresponding calculated value of 9.88 Å with a D_{6h} structure.

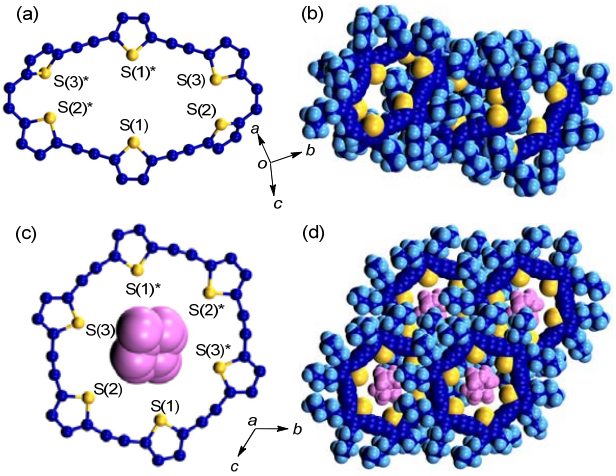

Fig. 9 (a) ORTEP diagram of **6T4A**. Butyl groups and hydrogen atoms omitted for clarity. (b) Entangled packing structure. (c) ORTEP diagram of **6T6A**. Butyl groups and hydrogen atoms omitted for clarity. A disordered hexane molecule is located in the center of the macroring. (d) Packing structure of **6T6A**.

Single crystals of *E*,*E*-**8T6A** and **8T8A** were obtained by recrystallization from hot benzene. As shown in Fig. 10, the cell parameters of *E*,*E*-**8T6A** are similar to those of **8T8A**.[43] *E*,*E*-**8T6A** and **8T8A** have a round structure and lie on a crystallographic center of symmetry (Fig. 10a and c). Although DFT calculations on unsubstituted *E*,*E*-**8T6A** and **8T8A** predicted planar C_{2h} and D_{8h} structure, respectively, *E*,*E*-**8T6A** adopts a nonplanar zigzag conformation (Fig. 10b), and **8T8A** adopts a slightly twisted oval structure (Fig. 10d and e). In the molecular packing, *E*,*E*-**8T6A** and **8T8A** form a honeycomb, columnar structure (Fig. 10c and f), and the butyl groups lie above and below the ring, filling the inner cavity of the neighboring rings.

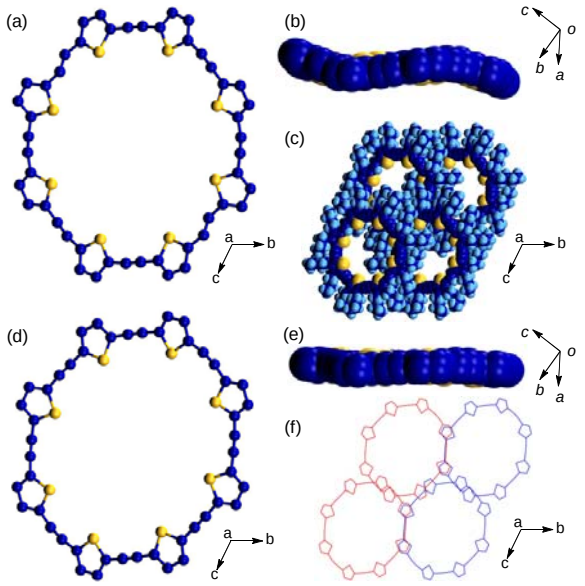

Fig. 10 (a) ORTEP diagram of *E*,*E*-**8T6A**. Butyl groups and hydrogen atoms omitted for clarity. (b) Side view and (c) packing structure of *E*,*E*-**8T6A**. (d) ORTEP diagram of **8T8A**. Butyl groups and hydrogen atoms omitted for clarity. (e) Side view and (f) packing structure of **8T8A**.

A single crystal of **10T8A** from chloroform–heptane contains 1.5 molar ratio of heptane to **10T8A**. As shown in Fig. 11, the 10 thiophene rings are arranged circularly with all the sulfur atoms in *s-cisoid* thiophene rings directed towards the inside.[44] This *s-cisoid* conformation makes the backbone curl and form a full circle. The intramolecular distances between the sulfur atoms in the opposite thiophene rings are 19.9 and 17.1 Å. The large cavity of **10T8A** is filled by central heptane and edging butyl groups of neighboring molecules, and the mutual sharing of the butyl groups of the neighboring molecules causes its frame to have a slightly bent chair-like conformation (Fig. 11b). Heptane molecules incorporated in the ring are considerably mobile, despite low-temperature X-ray analysis at –180 ºC. The X-ray analysis reveals that **10T8A** serves as a host molecule to alkane guests. Linear alkanes like hexane and octane are also incorporated in **10T8A** to form single crystals.

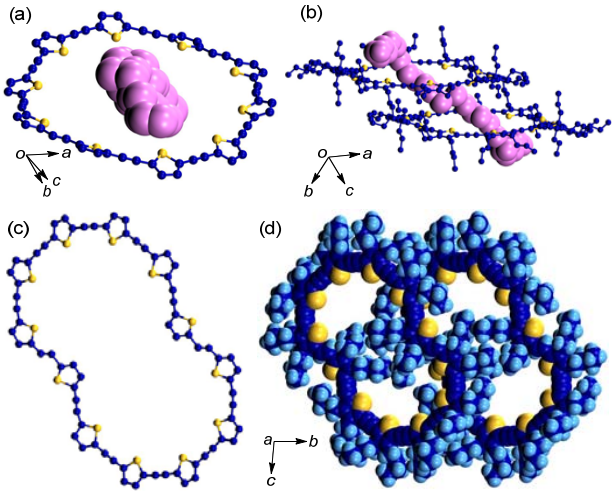

Fig. 11 (a) ORTEP diagram of **10T8A**·heptane. Butyl groups and hydrogen atoms omitted for clarity. (b) Crystal packing of **10T8A**·heptane. (c) ORTEP diagram of **12T10A**. Butyl groups and hydrogen atoms omitted for clarity. (d) Crystal packing of **12T10A**.

A single crystal of **12T10A** suitable for X–ray analysis was obtained from chloroform–decane (Fig. 11). Although **10T8A** has a nearly circular shape with all its thiophene units in the *cisoid* form, **12T10A** composed of 12 thiophene units has a narrow "waist" with two thiophene units in the *transoid* conformation so as to fill the center of the cycle.[45] The resultant small cavities are filled with neighboring butyl groups, and **12T10A** has a slightly bent chair–like structure. As a result, the single crystal involves no solvent molecule.

3.4 Redox behavior of π-expanded oligothiophene macrocycles *m*T*n*A

All π-expanded oligothiophene macrocycles behave as π-donors with fairly low oxidation potentials, although linear oligo(thienylene-ethynylene)s exhibit lower π-donor ability than common linear oligothiophenes. Cyclic voltammetric (CV) analyses of **4T2A** and **6T4A** exhibit two-electron one-step reversible waves owing to the formation of aromatic 22π and 34π dications **4T2A**$^{2+}$ and **6T4A**$^{2+}$, respectively, whereas *E*,*E*-**8T6A**, **10T8A**, and **12T10** show one-electron four-step, three-step, and two-step reversible waves, respectively, indicating intramolecular cation-cation interaction. Other giant macrocycles such as **15T12A**–**30T24A** and **18T15A**–**30T25A** show two reversible waves like linear long oligothiophenes. Therefore, smaller macrocycles exhibit stronger electronic interaction corresponding to on-site Coulombic repulsion, but macrocycles larger than a 90π system show only a small on-site Coulombic repulsion in their polycationic states. Interestingly, **9T6A**$^{2+}$, a 52π dication, indicated biradical cation character. Since the ESR spectrum of **9T6A**$^{\cdot+}$ (g = 2.0024 at 7 °C) is similar to that of **9T6A**$^{2+}$ (g = 2.0026 at 7 °C) (Fig. 12), the biradical state of **9T6A**$^{2+}$ is nearly equivalent to that of two independent monoradicals having a small exchange interaction.

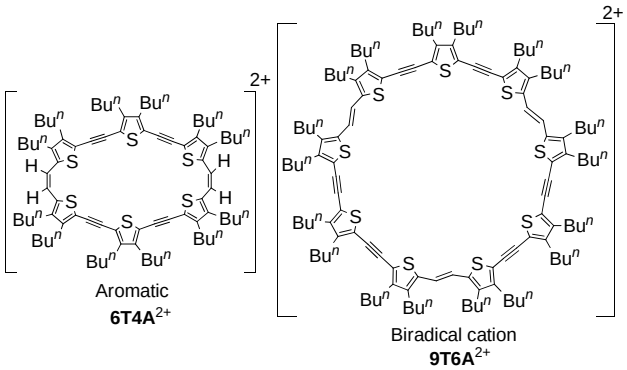

Fig. 12 Aromatic **6T4A**$^{2+}$ and biradical cation **9T6A**$^{2+}$.

Oligo- and polythiophenes are easily oxidized by electron acceptors to form the corresponding electroconductive radical salts. Important concepts for realizing high electrical conductivity are π–π stacking and π-dimer formation of cationic species derived from oligo- and polythiophenes. Although linear poly(thienylene–ethynylene)s seem to produce no electroconductive cationic species owing to difficulty in the formation of stable cationic species, macrocyclic oligothiophenes ***m*T*n*A** produce stable cationic species by oxidation and hence can form an electroconductive oxidation state. Actually, doping of **10T8A**, **15T12A**, and **20T16A** with iodine vapor resulted in the formation of black materials with moderate conductivities (**10T8A**: σ_{rt} = 1.86 × 10^{-3} Scm^{-1};

15T12A: σ_{rt} = 2.63 × 10^{-3} Scm^{-1}; **20T16A**: σ_{rt} = 2.03 × 10^{-3} Scm^{-1}, measured by 2 probe method).[47] Electrical conductivities of all the black materials increased after exposing **10T8A**, **15T12A**, and **20T16A** to iodine vapor for 5–70 min, though these conductivities gradually decreased to less than one-half of their maximum values on further exposure.

3.5 Polymorphism in 6T4A

One of the most interesting property of butyl-substituted π-expanded oligothiophenes is the polymorphism of **6T4A**.[42] As shown in Fig. 13, single crystals of **6T4A** corresponding to the X-ray structure (Fig. 9a) melted at 176 °C in the first heating process (blue line), determined by using differential scanning calorimetry (DSC) analysis. When cooled to room temperature, **6T4A** formed an amorphous solid. However, in the second heating process, **6T4A** showed an exothermic process (red line in the inset) at 80 °C to form crystals that melted at 139 °C, and in the third heating process, an exothermic process with a melt memory effect (green line in the inset) occurred at 83 °C to form crystals that melted again at 139 °C. Based on the analysis of the exothermic process by changing the heating and cooling rates, it was concluded that the difference of the exothermic temperature (inset in Fig. 13) was due to the thickness of the sample on the surface. Thus, **6T4A** has three solid state structures: single crystal, lamellar film (**LC-6T**), and amorphous film (**AF-6T**). This polymorphism was only observed for **6T4A** due to the number of stable conformations in the solid state, whereas the cast films of **6T6A**, **9T5A**, and related macrocycles formed amorphous solids and exhibited decomposition without showing a melting point. Since crystal structures should be ordered in the crystal lattice, **6T4A** adopts a twisted structure in the single crystal. However, the formation of an edge-on structure is favorable on the surface through π–π stacking interaction, and consequently, it was assumed that **6T4A** adopts a lamellarly aligned structure on the glass and metal surfaces.

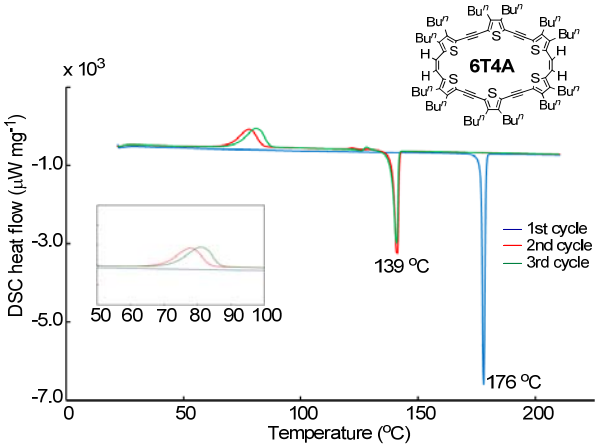

Fig. 13 DSC analysis of **6T4A** (2 °C/min). The inset shows the region 50 < T < 100 °C. Reproduced with permission from ref. 42. Copyright 2014 American Chemical Society.

Polymorphs of **6T4A** have different optical and electronic properties such as absorption and emission spectra, XRD patterns, FET behavior, and electrical conductivity of **AF-6T** and **LC-6T** on the surfaces of glass and metal plates.[42] The absorption and emission spectra of **LC-6T** (λ_{max} 418 and λ_{em} 674 nm) were redshifted compared to those of **AF-6T** (λ_{max} 384 and λ_{em} 607 nm) due to an increase in the π-π interactions (Fig. 14a). The colors of **AF-6T** and **LC-6T** are orange and reddish orange, respectively (Fig. 14b and d), consistent with the absorption spectra. The colors of **AF-6T** and **LC-6T** under UV-light (λ = 254 nm) were also different (Fig. 14c and e), and **AF-6T** fluoresced, whereas **LC-6T** only exhibited weak emission. The π–π stacked structure of **LC-6T** showed FET properties (μ = 2.8 × 10^{-3} $cm^2V^{-1}s^{-1}$, I_{on}/I_{off} = 10^4, and *V*th = –4.7 V) and an increased conductivity (σ_{rt} = 4.0 × 10^{-7} Scm^{-1}) compared with that of **AF-6T** (σ_{rt} = 2.6 × 10^{-10} Scm^{-1}). Furthermore, after doping with iodine, the conductivities of **AF-6T** and **LC-6T** (2.5 × 10^{-5} and 1.1 × 10^{-2} Scm^{-1}, respectively) were higher than those of the corresponding neutral films, and the conductivity of doped **LC-6T** was 440-times higher than that of doped **AF-6T**.

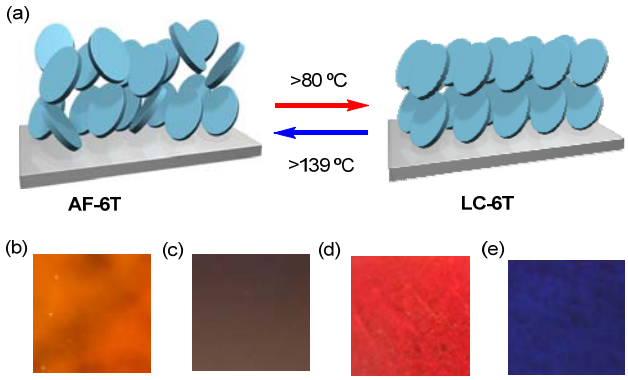

Fig. 14 (a) Schematic representation of the polymorphism of amorphous film **AF-6T** and lamellarly stacked crystalline film **LC-6T** on substrate surfaces. (b) The color of **AF-6T**, (c) the color of **AF-6T** under UV-light irradiation (λ = 254 nm), (d) the color of **LC-6T**, and (e) the color of **LC-6T** under UV-light irradiation (λ = 254 nm). Reproduced with permission from ref. 42. Copyright 2014 American Chemical Society.

3.6 Nanostructured polymorphs of *E,E*-8T6A and 15T9A–30T24A

A conformationally restricted structure stabilizes various mesophases,[48] and hence fibrous structure of *E,E*-**8T6A** precipitated from solution.[43] As shown in Fig. 15, fibers, rods, and square tubes of *E,E*-**8T6A** precipitated from hexane/benzene (Fig. 15a), chloroform (Fig. 15b), and benzene/diisopropyl ether (IPE) (Fig. 15c and d). None of these fibers, rods, and square tubes of *E,E*-**8T6A** contained any solvent. The XRD patterns for the fibers corresponded to those for a 1D structure, whereas the XRD patterns for the rods and square tubes indicated microcrystalline structures.

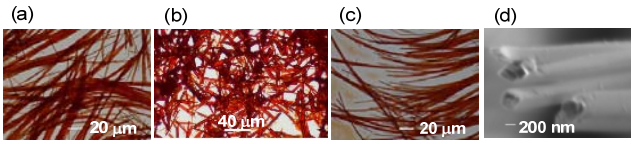

Fig. 15 Optical images of (a) fibers from hexane/benzene, (b) rods from chloroform, and (c) square tubes from benzene/IPE. (d) SEM image of the square tube of *E,E*-**8T6A**. Reproduced with permission from ref. 43. Copyright 2015 American Chemical Society.

Giant macrocycles **10T8A–30T24A** exhibit a ring-size dependence of the morphology.[44] As shown in Fig. 11, **10T8A** formed single crystals; however, **15T12A** formed microcrystals and fibers from ethyl acetate/octane (Fig. 16a), and **20T16A**

formed fibers from ethyl acetate/chloroform (Fig. 16b). In contrast, **25T20A** and **30T24A** formed nanoparticles from ethyl acetate/chloroform (Fig. 16c and d). Unlike single crystals of **10T8A**, none of these polymorphs of **15T12A**–**30T24A** contained any solvent.

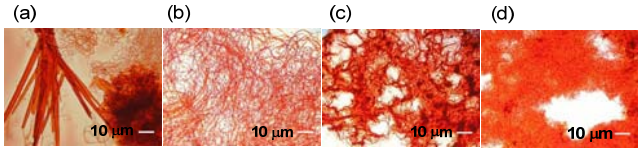

Fig. 16 Microscopic images of (a) **15T12A**, (b) **20T16A**, (c) **25T20A**, and (d) **30T24A**. Reproduced with permission from ref. 44. Copyright 2006 American Chemical Society.

3.7 Photoisomerization between *E,E*-8T6A and *Z,Z*-8T6A

In solution, *E,E*-**8T6A** and *Z,Z*-**8T6A** isomerized to *Z,Z*-**8T6A** and *E,E*-**8T6A**, respectively, by irradiation.[43] As shown in Fig. 17, *E,E*-**8T6A** and *Z,Z*-**8T6A** exhibit different UV-vis spectra. In other words, irradiation of orange solutions of *E,E*-**8T6A** in cyclohexane, chloroform, toluene, and benzene with green light (λ = 525 nm) produced *Z,Z*-**8T6A** nearly quantitatively. On the other hand, irradiation of a yellow solution of *Z,Z*-**8T6A** in cyclohexane with UV light (λ = 365 nm) produced *E,E*-**8T6A** in 96% yield with a trace amount of *E,Z*-**8T6A**, and only *E,E*-**8T6A** crystalized from the mixture of products. In summary, **8T6A** exhibited reversible photochromic behavior between two geometric isomers in solution.

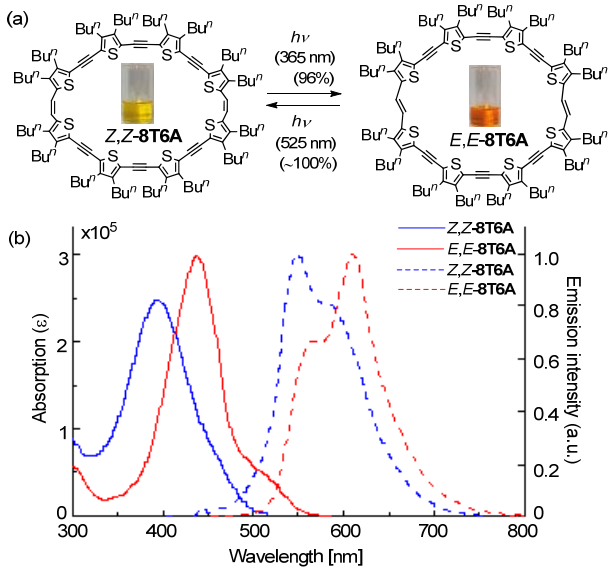

Fig. 17 (a) Photochromism between *Z,Z*-**8T6A** and *E,E*-**8T6A**. (b) Absorption and emission spectra of *Z,Z*-**8T6A** and *E,E*-**8T6A** in cyclohexane at 25 ºC. Reproduced with permission from ref. 43. Copyright 2015 American Chemical Society.

As noted above, *Z,Z*-**8T6A** produced no crystals from common organic solvents but formed an amorphous film on glass and metal surfaces. Interestingly, the amorphous film of *Z,Z*-**8T6A** photoisomerized almost quantitatively to the amorphous film of *E,E*-**8T6A** by irradiation with UV light at 365 nm,[43] although the amorphous film of *E,E*-**8T6A** could not be prepared from solutions of *E,E*-**8T6A**. Photoisomerization of the amorphous film of *E,E*-**8T6A** at 480 nm afforded the amorphous film of *Z,Z*-**8T6A** again in ca. 60% yield. Scanning tunneling microscope (STM) images of *E,E*-**8T6A** and *Z,Z*-**8T6A** at the solid–liquid interface[49] show that both *E,E*-**8T6A** and *Z,Z*-**8T6A** self-assembled in a hexagonal close-packed monolayer, and the unit cell parameters for the *E,E*-**8T6A** structure were larger than those for *Z,Z*-**8T6A** (Fig. 18). The contrasts of the moieties assigned to the macrocycle core were consistent with the optimized DFT structures, and *E,E*-**8T6A** appeared as a circular contour (Fig. 18a and b), whereas *Z,Z*-**8T6A** appeared as an ellipsoidal one (Fig. 18c and d). Photoisomerization of *Z,Z*-**8T6A** to *E,E*-**8T6A** and *E,E*-**8T6A** to *Z,Z*-**8T6A** upon irradiation at 365 and 550 nm, respectively, was observed at the solid–liquid interface using the STM.

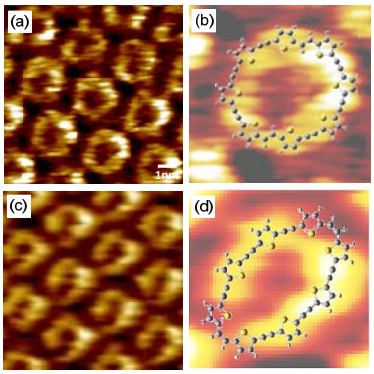

Fig. 18 STM height images of a hexagonal network of (a) *E,E*-**8T6A**, unit cell: a = (2.97 ± 0.03) nm, b = (2.95 ± 0.03) nm, θ = (59 ± 3)°, U_t = 1.12 V, I_t = 58 pA and (b) image of *E,E*-**8T6A** from B3LYP calculation. (c) *Z,Z*-**8T6A**, unit cell: a = (2.83 ± 0.11) nm, b = (2.83 ± 0.09) nm, θ = (60 ± 1)°, U_t = 1.14 V, I_t = 57 pA, (d) image of *Z,Z*-**8T6A** from B3LYP calculation. Reproduced with permission from ref. 43. Copyright 2015 American Chemical Society.

3.8 Nonlinear optical properties and light harvesting behavior

Absorption and emission spectra of macrocycles **10T8A**–**30T24A** and **12T10A**–**30T25A** measured in dichloromethane show an important feature. As has been reported previously, a series of linear oligo(thienylene-ethynylene)s up to 16-mer exhibited near saturation for the absorption maximum at the 8-mer stage.[50] Therefore, doubling the conjugation length from 8-mer to 16-mer causes little change in the absorption maximum. In contrast, **10T8A**–**30T24A** and **12T10A**–**30T25A** exhibited a redshift of their longest absorption maxima with increasing ring size (Fig. 19). A linear relationship between the longest absorption maxima (eV) and the reciprocal of the number of thiophenes (1/n) in **10T8A**–**30T24A** suggests that the considerable π–π overlapping is maintained (Fig. 19a). Recent studies on the exciton delocalization of linear and cyclic oligothiophenes exhibited that a cyclic geometry of **10T8A** reduces conformational disorder of the chain, and a rigid planar structure thus formed effectively delocalizes exciton over the molecular backbone.[51]

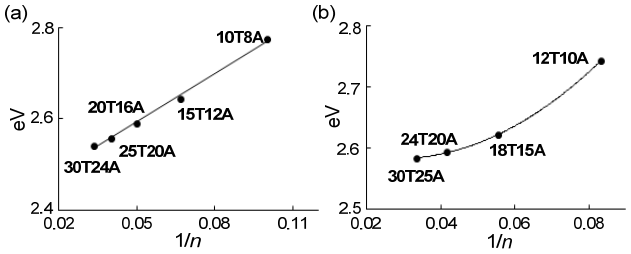

Fig. 19 Relationship between the longest absorption maxima (eV) and the number of thiophenes (*n*). (a) **10T8A**–**30T24A**. (b) **12T10A**–**30T25A**.

Of these oligothiophene macrocycles, the two-photon properties of **12T10A**–**30T25A** were chosen for investigation. The two-photon absorption cross section (δ_{max}) is **12T10A**: 15,100 GM, **18T15A**: 66,700 GM, **24T20A**: 82,600 GM, **30T25A**: 107,800 GM. Therefore, the increasing ring size and π-character from **12T10A** (72π) to **18T15A** (108π), **12T10A** to **24T20A** (144π), and **12T10A** to **30T25A** (180π) result in respectively 4.4-, 5.5-, and 7.1-fold amplifications of the maximum two-photon absorption cross section (Fig. 20). These large enhancements in two-photon absorption cross section are due to intramolecular interactions between these giant macrocycles. It should be noted that the increasing π-conjugation leads to an increase in the two-photon absorption cross section with magnitudes as high as 100,000 GM in the visible spectral region. Interestingly, for the largest giant macrocycle **30T25A**, the initial localized excited state is followed by incoherent hopping to form the exciton delocalization along the whole ring (Fig. 20b).[52] As a result, the life time of the excited state of **30T25A** is extended. These experiments suggest that the initial delocalized state increases with ring size, a result comparable to the natural light-harvesting system.

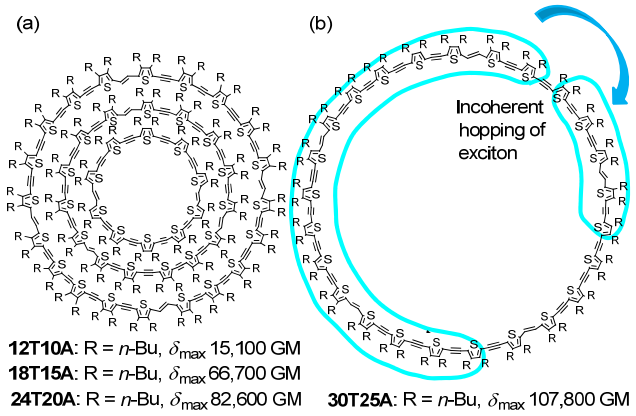

Fig. 20 Characteristic properties of **12T10A**–**30T25A**. (a) Large enhancements of two-photon absorption cross sections of **12T10A**, **18T15A**, and **24T20A**. (b) Incoherent hopping of exciton in the excited state of **30T25A** with large two-photon properties.

3.9 Formation of C_{60} complexes

Macrocycles with precise shapes and inner cavities form various kinds of C_{60}-containing complexes. Among them, convex-concave π-π interactions between the spherical C_{60} and π-conjugated tublar molecules play an important role in stabilizing inclusion complexes, whereas van der Waals interactions between C_{60} and macrocycles help to construct 1:1 inclusion complexes. Although van der Waals interactions are usually too weak to allow for the formation of stable complexes, *E,E*-**8T6A** and **8T8A** incorporate C_{60} in their inner cavities to form unique Saturn-like complexes using mainly van der Waals interactions between C_{60} and the sulfur atoms of oligothiophene 8-mers.

In contrast to the weak interactions of *E,E*-**8T6A** and **8T8A** with C_{60} in solution, these macrocycles formed stable C_{60}-complexes in the solid state.[43] Single crystals of *E,E*-**8T6A**$\supset C_{60}$ and **8T8A**$\supset C_{60}$ were obtained by crystallization of *E,E*-**8T6A** and **8T8A** with C_{60}, respectively, in hot toluene, and their Saturn-like structures were determined by using X-ray analysis (Fig. 21). In *E,E*-**8T6A**$\supset C_{60}$, the face-to-face S···S distances (13.607(2)–14.661(3) Å, average S···S distance: 13.99 Å) indicate that the oligothiophene ring is nearly circular, and the short S···S distances (13.607 and 13.661 Å) are 1.0% shorter than the sum (13.72 Å) of the van der Waals radii of the sulfur atoms (3.70 Å) and C_{60} (10.02 Å). The short contacts between the sulfur atoms and C_{60} stop the rotation of C_{60}, which is different from complexes with convex-concave π-π interactions in a ball bearing system.[11]

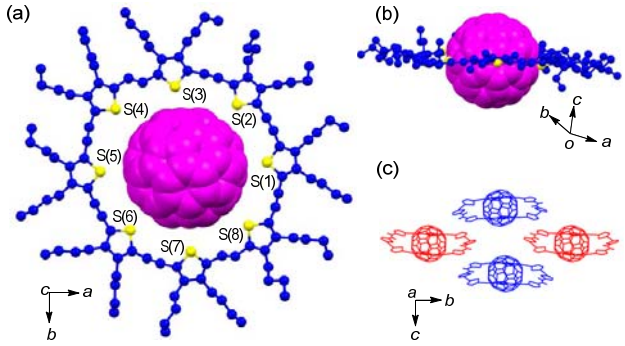

Fig. 21 X-ray structure of *E,E*-**8T6A**$\supset C_{60}$. (a) Top view, (b) side view, and (c) packing structure along the *a*-axis. Reproduced with permission from ref. 43. Copyright 2015 American Chemical Society.

Interestingly, **19a**, a nonplanar system, formed 1:2 complex with C_{60} in the single crystal (Fig. 22).[31] The two C_{60} molecules were incorporated in the cavities on each side of **19a** with 1,3-alternating geometry. Opposite pairs of DTT rings incorporate one C_{60} on each side of the macrocycle. The ring of **19a** captured the C_{60} through π–π interactions as well as sulfur–π contacts. Since the crystal has an S_4 axis in the center of the macrocycle, the cavities are crystallographically identical, which gives rise to the "Janus-head" in **19a**.

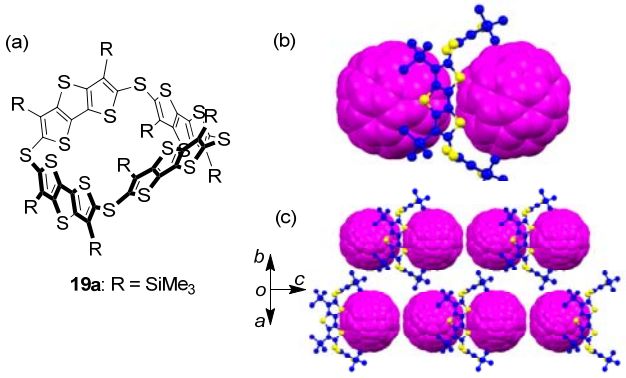

Fig. 22 (a) Nonplanar π-expanded oligothiophene macrocycle **19a**. X-ray structure of **19a**·$(C_{60})_2$: (b) side view and (c) a columnar array along the *c*-axis. *o*-Xylene omitted for clarity.

4. Conclusion

Numerous shape-persistent π-conjugated macrocycles have been constructed and investigated to satisfy synthetic challenges and theoretical interests. Among them, π-expanded oligothiophene macrocycles are redox-active π-donors with

characteristic optical and electronic properties. Therefore, molecular design and synthesis of these molecules can realize their remarkable multifunctional properties in solution and the solid state. First, oligothiophene macrocycles exhibit a larger effective conjugation length than oligophenylene macrocycles, and large macrocycles can often be treated as a fully conjugated system. This extended π-conjugation makes giant macrocyclic oligothiophenes extremely attractive. Especially, π-expanded oligothiophene macrocycles composed of 2,5-thienylene, ethynylene, and vinylene units show very effective cyclic conjugation, because these macrocycles possess almost no steric repulsion between neighboring thiophene rings, and because torsional strain in the small or large ring is diminished by bending of ethynylene and/or vinylene units without significant loss of molecular stability. Second, inner cavities of oligothiophene macrocycles are easily adjustable to guest molecule through selecting numbers of 2,5-thienylene, ethynylene, and vinylene units. Thus, the cavity size of macroring is adjusted to fullerenes to produce Saturn-like complexes. Furthermore, π-expanded oligothiophene macrocycles exhibit unique redox behavior, electric conductivity, polymorphism, photochromism, nonlinear optical properties, and light harvesting behavior, and therefore, these macrocycles find functions in mass use devices, if full advantages can be taken of these systems. Finally, π-expanded oligothiophene macrocycles face the new century as one of the target molecules to be exploited in depth.

Acknowledgements

This work was supported by a Grant-in-Aid for Scientific Research from the Ministry of Education, Culture, Sports, Science and Technology, Japan and by CREST and SICP of JST (Japan Science and Technology Corporation). We would like to thank Prof. Takeshi Kawase (University of Hyogo) for the X-ray data of **32**.

Notes and references

Department of Chemistry, Graduate School of Science and Engineering, Tokyo Metropolitan University, Hachioji, Tokyo 192-0397, Japan
E-mail: Iyoda@tmu.ac.jp

1 M. Iyoda, J. Yamakawa, and M. J. Rahman, *Angew. Chem. Int. Ed.*, 2011, **50**, 10522–10553.
2 J. A. Marsden, G. J. Palmer, and M. M. Haley, *Eur. J. Org. Chem.*, 2003, **13**, 2355–2369.
3 T. Kawase and H. Kurata, *Chem. Rev.*, 2006, **106**, 5250–5273.
4 M. V. Martínez-Díaz, G. De La Torre, and T. Torres, *Chem. Commun.*, 2010, **46**, 7090-7108.
5 T. F. A. De Greef, M. M. J. Smulders, M. Wolffs, A. P. H. J. Schenning, R. P. Sijbesma, and E. W. Meijer, *Chem. Rev.*, 2009, **109**, 5687–5754.
6 T. Kudernac, S. Lei, J. A. A. W. Elemans, and S. De Feyter, *Chem. Soc. Rev.*, 2009, **38**, 402–421.
7 K. Tahara and Y. Tobe, *Chem. Rev.*, 2006, **106**, 5274–5290.
8 Y. Miller, B. Ma, and R. Nussinov, *Chem. Rev.*, 2010, **110**, 4820–4838.
9 T. Kawase, H. R. Darabi, and M. Oda, *Angew. Chem. Int. Ed.*, 1996, **35**, 2664–2666.
10 R. Jasti, J. Bhattacharjee, J. B. Neaton, and C. R. Bertozzi, *J. Am. Chem. Soc.*, 2008, **130**, 17646–17647.
11 H. Isobe, S. Hitosugi, T. Yamasaki, R. Iizuka, *Chem. Sci.*, 2013, **4**, 1293-1297.
12 Y. Nakanishi, H. Omachi, S. Matsuura, Y. Miyata, R. Kitaura, Y. Segawa, K. Itami, and H. Shinohara, *Angew. Chem. Int. Ed.*, 2014, **53**, 3102–3106, and references cited therein.
13 S. Yamago, E. Kayahara, and T. Iwamoto, *Chem. Rec.*, 2014, **14**, 84–100, and references cited therein.
14 P. J. Evans, E. R. Darzi, and R. Jasti, *Nature Chem.*, 2014, **6**, 404–408, and references cited therein.
15 T. Nishiuchi, X. Feng, V. Enkelmann, M. Wagner, and K. Müllen, *Chem. Eur. J.*, 2012, **18**, 16621–16625.
16 E. Kayahara, T. Kouyama, T. Kato, H. Takaya, N. Yasuda, and S. Yamago, *Angew. Chem. Int. Ed.*, 2013, **52**, 13722–13726.
17 M. R. Golder, B. M. Wong, and R. Jasti, *Chem. Sci.*, 2013, **4**, 4285–4291.
18 T. Iwamoto, Y. Watanabe, T. Sadahiro, T. Haino, and S. Yamago, *Angew. Chem. Int. Ed.*, 2011, **50**, 8342–8344.
19 J. Xia, J. W. Bacon, and R. Jasti, *Chem. Sci.*, 2012, **3**, 3018–3021.
20 T. Kawase, K. Tanaka, N. Shiono, Y. Seirai, and M. Oda, *Angew. Chem. Int. Ed.*, 2004, **43**, 1722–1724.
21 J. Krömer, I. Rios-Carreras, G. Fuhrmann, C. Musch, M. Wunderlin, T. Debaerdemaeker, E. Mena-Osteritz, and P. Bäurele, *Angew. Chem. Int. Ed.*, 2000, **39**, 3481–3486.
22 A. Mishra, C.-Q. Ma, J. L. Segura, P. Bäurele, Functional oligothiophene-based materials: nanoarchitectures and application pp1, in Handbook of Thiophene-based Materials, eds by I. F. Perepichka, D. F. Perepichka, Wiley, London (2009), and references cited therein.
23 E. Mena-Osteritz, and P. Bäurele, *Adv. Mater.*, 2001, **13**, 243–246.
24 G. Fuhrmann, T. Debaerdemaeker, and P. Bäurele, *Chem. Commun.*, 2003, 948–949.
25 F. Zhang, G. Götz, H. D. K. Winkler, C. A. Schalley, and P. Bäurele, *Angew. Chem. Int. Ed.*, 2009, **48**, 6632–6635.
26 F. Zhang, G. Götz, E. Mena-Osteritz, M. Weil, B. Sarkar, W. Kaim, and P. Bäurele, *Chem. Sci.*, 2011, **2**, 781–784.
27 F. Sannicolò, P. R. Mussini, T. Benincori, R. Cirilli, S. Abbate, S. Arnaboldi, S. Casolo, E. Castiglioni, G. Longhi, R. Martinazzo, M. Panigati, M. Pappini, E. Q. Procopio, and S. Rizzo, *Chem. Eur. J.*, 2014, **20**, 15298–15302.
28 K. Asai, A. Fukazawa, and S. Yamaguchi, *Chem. Commun.*, 2015, **51**, 6096–6099.
29 J. A. Marsella, I. T. Kim, and F. Tham, *J. Am. Chem. Soc.*, 2000, **122**, 974–975.
30 H. Ito, Y. Mitamura, Y. Segawa, K. Itami, *Angew. Chem. Int. Ed.*, 2015, **54**, 159–163.
31 R. Inoue, M. Hasegawa, T. Nishinaga, K. Yoza. and Y. Mazaki, *Angew. Chem. Int. Ed.*, 2015, **54**, 2734–2738.
32 Z. Hu, J. L. Atwood, and M. P. Cava, *J. Org. Chem.*, 1994, **59**, 8071-8075.
33 E. Vogel, M. Pohl, A. Herrmann, T. Wiss, C. Konig, J. Lex, M. Gross, and J. P. Gisselbrecht, *Angew. Chem. Int. Ed.*, 1996, **35**, 1520–1524.
34 M. Mayor and C. Didschies, *Angew. Chem. Int. Ed.*, 2003, **42**, 3176–3179.
35 Y. Ie, T. Hirose, and Y. Aso, *J. Mater. Chem.*, 2009, **19**, 8169–8175.

36 G.-B. Pan, X.-H. Cheng, S. Höger, and W. Freyland, *J. Am. Chem. Soc.*, 2006, **128**, 4218–4219.
37 M. Iyoda, *Pure Appl. Chem.*, 2010, **82**, 831–841.
38 M. Iyoda, M. Hasegawa, and H. Enozawa, *Chem. Lett.*, 2007, **36**, 1402–1407.
39 T. Kawase, H. R. Darabi, R. Uchiyama, and M. Oda, *Chem. Lett.*, 1995, **24**, 499–500.
40 M. Iyoda, P. Huang, T. Nishiuchi, M. Takase, and T. Nishinaga, *Heterocycles*, 2011, **82**, 1143–1149.
41 T. Nishiuchi and M. Iyoda, *Chem. Rec.*, 2015, **15**, 329–346.
42 M. Iyoda, K. Tanaka, H. Shimizu, M. Hasegawa, T. Nishinaga, T. Nishiuchi, Y. Kunugi, T. Ishida, H. Otani, H. Sato, K. Inukai, K. Tahara, and Y. Tobe, *J. Am. Chem.* Soc. 2014, **136**, 2389–2396.
43 H. Shimizu, J. D. Cojal González, M. Hasegawa, T. Nishinaga, T. Haque, M. Takase, H. Otani, J. P. Rabe, and M. Iyoda, *J. Am. Chem. Soc.*, 2015, **137**, 3877–3885.
44 K. Nakao, M. Nishimura, T. Tamachi, Y. Kuwatani, H. Miyasaka, T. Nishinaga, and M. Iyoda, *J. Am. Chem. Soc.*, 2006, **128**, 16740–16747.
45 M. Williams-Harry, A. Bhaskar, G. Ramakrishna, T. Goodson, III, M. Imamura, A. Mawatari, K. Nakao, H. Enozawa, T. Nishinaga, and M. Iyoda, *J. Am. Chem. Soc.*, 2008, **130**, 3252–3253.
46 A. Orita and J. Otera, *Chem. Rev.*, 2006, **106**, 5387–5412.
47 M. Hasegawa and M. Iyoda, *Chem. Soc. Rev.*, 2010, **39**, 2420–2427.
48 Y. Hanai, M. J. Rahman, J. Yamakawa, M. Takase, T. Nishinaga, M. Hasegawa, K. Kamada, and M. Iyoda, *Chem. Asian J.*, 2011, **6**, 2940–2945.
49 C. Seifert, D. Skuridina, X. Dou, K. Müllen, N. Severin, and J. P. Rabe, *Phys. Rev. B*, 2009, **80**, 245429, and references cited therein.
50 M. Melucci, G. Barbarella, M. Zambianchi, P. D. Pietro, and A. Bongini, *J. Org. Chem.*, 2004, **69**, 4821–4828, and references cited therein.
51 P. Kim, K. H. Park, W. Kim, T. Tamachi, M. Iyoda, and D. Kim, *J. Phys. Chem. Lett.*, 2015, **6**, 451-456.
52 J. E. Donehue, O. P. Varnavski, R. Cemborski, M. Iyoda, and T. Goodson III, *J. Am. Chem. Soc.*, 2011, **133**, 4819–4828.